Computational Materials Science 187 (2021) 110119

Contents lists available at ScienceDirect

Computational Materials Science

journal homepage: www.elsevier.com/locate/commatsci

Machine learned metaheuristic optimization of the bulk heterojunction morphology in P3HT:PCBM thin films

Joydeep Munshi [a], Wei Chen [b], TeYu Chien [c], Ganesh Balasubramanian [a,*]

[a] Department of Mechanical Engineering & Mechanics, Lehigh University, Bethlehem, PA 18015, United States
[b] Department of Mechanical Engineering, Northwestern University, Evanston, IL 60208, United States
[c] Department of Physics & Astronomy, University of Wyoming, Laramie, WY 82071, United States

ARTICLE INFO

Keywords:
P3HT:PCBM
Cuckoo Search
Support vector machines
Coarse-grained molecular dynamics
Pareto frontier
Organic solar cells

ABSTRACT

We discuss results from a machine learned (ML) metaheuristic cuckoo search (CS) optimization technique that is coupled with coarse-grained molecular dynamics (CGMD) simulations to solve a materials and processing design problem for organic photovoltaic (OPV) devices. The method is employed to optimize the composition of donor and acceptor materials, and the thermal annealing temperature during the morphological evolution of a polymer blend active layer composed of poly-(3-hexylthiophene) (P3HT) and phenyl-C61-butyric acid methyl ester (PCBM), for an increased power conversion efficiency (PCE). The optimal solutions, which are in qualitative agreement with earlier experiments, identify correlation between the design variables that contributes to an enhanced material performance. The framework is extended to multi-objective design (MOCS-CGMD) to attain a Pareto optimality for the blend morphology, and enhance concurrently the exciton diffusion to charge transport probability and the ultimate tensile strength of the material. The predictions reveal that a higher annealing temperature enhances the exciton diffusion to charge transport probability, while a PCBM weight fraction between 0.4 and 0.6 increases the tensile strength of the underlying blend morphology.

1. Introduction

Polymer-based materials have been employed for organic photovoltaic (OPV) applications due to their low-temperature solution processability, inherent flexibility and environ-friendly synthesis and electricity generation [1–3]. Organic solar cells (OSC) consisting of an interpenetrating mixture of electron donor and acceptor materials exhibit the most promising photoactive layer (*a.k.a.* bulk heterojunction) due to their notable ability to convert absorbed photon to charge carriers, resulting in high power conversion efficiency (PCE) [4]. Numerous experimental and computational investigations in the past decade have confirmed the correlation between PCE and the underlying nanomorphology by correlating the processing to structure to performance (PSP) [5–10]. Although extensive research have raised the efficiency of polymer-based OSCs to ~ 10% [11–13], recent efforts suggest the need for novel organic materials as well as new active layer architectures, such as tandem BHJ active layers that have exhibited exemplary PCE > 15% [14,15]. On the other hand, the thermomechanical stability of typical BHJ blends is essential because the elasto-morphology steers the ultra-flexible nature of these thin films [16–21]. Thus, a multi-objective optimization is indispensable to design processing-driven morphology for the targeted device performance as well as mechanical stability. To address this need, we present a data-enabled metaheuristic optimization scheme, which encapsulates coarse-grained molecular dynamics (CGMD) simulations, to recommend processing and material considerations for designer OSCs with targeted properties. In particular, exciton diffusion to charge transport probability and the ultimate tensile strength under an applied deformation strain are considered as the objective functions. Our results, as discussed below, demonstrate significant acceleration of materials design relative to contemporary methods.

Intractable (*a.k.a.* black-box) objective functions are difficult to optimize using gradient based algorithms such as gradient descent or conjugate gradient [22,23]. Nature-inspired metaheuristic algorithms, on the other hand, are an alternative to rapidly converge the black-box functions to their respective global solutions [24–27]. Despite the extensive use of genetic algorithm (GA) [24] and particle swarm optimization (PSO) [25] algorithm for applications in manufacturing, production and design, a recently developed optimization technique called Cuckoo Search (CS) [26] enables an efficient and rapid convergence to

* Corresponding author at: Packard Laboratory 561, 19 Memorial Drive West, Bethlehem, PA 18015, United States.
E-mail address: bganesh@lehigh.edu (G. Balasubramanian).

https://doi.org/10.1016/j.commatsci.2020.110119
Received 6 August 2020; Received in revised form 29 September 2020; Accepted 11 October 2020

the global solution, making it superior than GA and PSO for multimodal design problems such as optimizing processing-driven nanomorphology in a typical OSC active layer. Deb *et. al.* [28] extended the traditional CS algorithm to facilitate multi-objective optimization (MOCS). In brief, CS search mimics obligate brood parasitism of female cuckoo species that often chooses nests of a host bird which has just laid its own eggs. The new born cuckoo chick, once incubated, evicts the host eggs out of the nest to increase its food share [29]. This imitation strategy of parasitic cuckoo species can be implemented as an optimization strategy to various applications, especially for problems with the intractable objective functions. Additionally, the CS algorithm [26] adopts Lévy flights module to search the parametric landscape that efficiently juxtaposes with the traditional Gaussian process random walks [30] for rapid convergence to globally optimal solutions.

We integrate the CS scheme with classical CGMD simulations to optimize representative design parameters such as composition of donor and acceptor materials and thermal annealing temperature for targeted properties. The results from the CGMD simulations of a typical solvent-free mixture of poly-(3-hexyl-thiophene) (P3HT) and phenyl-C_{61}-butyric acid methyl ester (PCBM) that compose the BHJ morphology provide feedback to the CS scheme iteratively to facilitate the search for the optimal solution. The CS-CGMD method, discussed herein, is extended to a bivariate and multi-objective optimization scheme (MOCS-CGMD) based on the CS-MD framework established in a previous effort [31].

2. Design methods

2.1. Cuckoo search algorithm

The original CS single objective optimization [26], where each egg in a nest is considered as a possible solution, is governed by a set of idealized rules:

1. At a given time, a cuckoo lays one egg and deposits it in a random nest.
2. The best nest consisting of a high-quality egg (solution) is passed on to the next generation.
3. An alien egg is discovered by a host bird with probability $p_a \in [0,1]$. If the host bird identifies an alien egg it will get rid of it by either abandoning the nest or evicting the egg out of the nest. The total number of nests in each generation remains constant.

The MOCS with N different objectives can be achieved by adapting the first and third rules [28]:

- At a given time, each cuckoo lays N eggs corresponding to N possible solutions and deposits them in a random nest.
- Each nest will be discarded with probability $p_a \in [0, 1]$ and a new nest with N eggs will be generated.

CS leverages the efficient global Lévy flight mechanism whose step length is determined from a Lévy distribution, $L(s,\lambda) = \frac{\lambda\Gamma(\lambda)\sin(\frac{\pi\lambda}{2})}{\pi s^{1+\lambda}}, (s \gg 0)$ where $\Gamma(\lambda)$ is the gamma function. Consequently, the global random walk is represented as $x_i^{t+1} = x_i^t + \alpha L(s,\lambda)$ where $\alpha > 0$ is the step-size scaling factor related to the boundary of the defined design landscape and x_i^{t+1}, x_i^t are eggs (solutions) from the consecutive generation. On the other hand, the progression of nests by local random walk is represented as $x_i^{t+1} = x_i^t + \alpha s \otimes H(p_a - \varepsilon) \otimes (x_i^t - x_k^t)$where $H(x)$ is a Heaviside function, $\varepsilon$is a random number, x_i^t, x_k^t are solutions selected from random permutations and $\otimes$ represents entry wise product. We select the switching parameter $p_a = 0.2$ as the convergence of the CS optimization has been found to be minimally dependent on the choice [31]. We examine two cases with $n = 5$ and 10, to evaluate the differences in the computational performance of the optimization. The CS-CGMD scheme, illustrated in Fig. 1, involves optimizing one or more design variables for the targeted property such as the exciton diffusion to charge transport probability of a thin film active layer morphology. During each optimization generation, the CS-CGMD scheme compares different solutions amongst the different nests and retains a fraction of the best candidates. All the ill-performing solutions are replaced with newer alternatives from global and local explorations in the design space leveraging the efficient Lévy flights to eliminate the local saddle points.

Nevertheless, predictions from a large set of computationally-expensive CGMD simulations remain unutilized during the

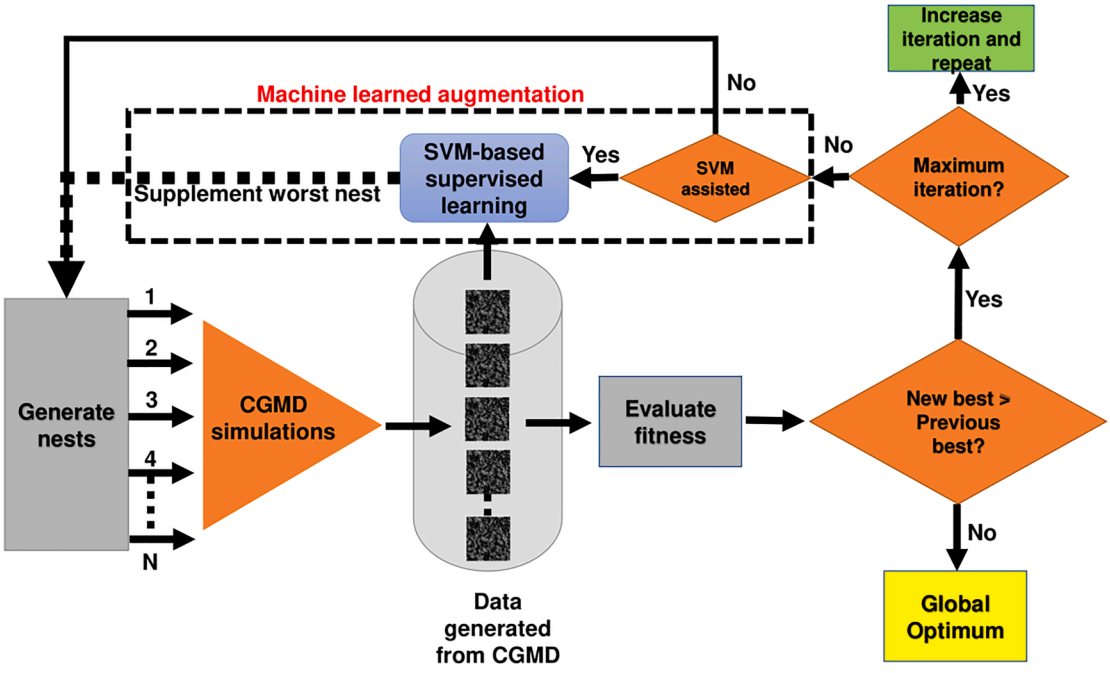

Fig. 1. Flowchart describing steps in a typical coupled Cuckoo Search-CGMD (CS-CGMD) algorithm. The dashed box represents the augmented machine learned exploration of the regions of interest (ROIs) to supplement ill-performed nests with newer alternatives during each CS optimization generation.

metaheuristic search. Inspired by the promise of machine learning (ML) in the device optimization [32] for the OPV applications, we data-enable the CS-CGMD scheme to predict the global solution leveraging morphological predictions from the gamut of the CGMD calculations. We augment the CS-CGMD with a ML-guided regression approach to streamline the choice of eggs during each optimization generation. A support vector machine (SVM), *a.k.a.* support vector regressor (SVR), with the radial basis function (RBF) fitting is applied to the results from CGMD simulations during each generation of the CS optimization. The response surface prediction from the SVM model during each training cycle is used to locate the region of interest (ROI). Next, the best prediction from the respective generations based on the SVM assisted supervised training is used to replace one of the worst performing nests from the preceding generation. Subsequently, following each generation of optimization, the training dataset is augmented with new CGMD predictions improving the overall analytic efficiency of the supervised learning. We designate that the SVM model has assisted a CS optimization run, if the SVM assisted egg results in superior properties for the material. In this SVM enabled CS-CGMD, as illustrated in Fig. 1, supervised learning is employed using SVR libraries implemented in Scikit-learn [33] composed with the Python language.

3. CGMD simulations

The Martini forcefield [5,34], extended to polymers, fullerene and benzene rings [35–37], are employed to model intermolecular interactions in the CGMD simulations of BHJ blend morphology consisting of P3HT, PCBM and Chlorobenzene (CB) molecules. While the CG model resolution can affect the calculated elastic properties and density, the solution processed BHJ layer from the three-site model [7] are found to concur with experiments [21]. The computational procedure adopted to mimic a typical spin-coating process to prepare P3HT: PCBM BHJ structure is described in detailed in our earlier reports [9,10,38] and provided as supplementary information. Nonequilibrium simulations are employed to model the mechanical deformation of thermally annealed BHJ blend under a constant velocity of deformation boundary condition along the longitudinal (*x*-) direction , following the recently developed protocol in our earlier effort [20]. GROMACS 2019.4 [39] is used for all the CGMD simulations and VMD 1.8.2 (Visual Molecular Dynamics) [40] for visualization of the molecular structures.

The objective functions in our CS-CGMD optimization algorithm is implemented from the evaluation of exciton diffusion to charge transport probability (*P*) and ultimate tensile strength (UTS). The molecular trajectories from the CGMD simulations are utilized to analyse the exciton diffusion to charge transport probability (*P*) and the UTS of the BHJ morphology under constant deformations. Exciton diffusion, charge dissociation and charge transport in BHJ layers depend on three key morphological features, *viz.*, average domain size, interfacial area and percolation ratio. Despite the low photon absorption in fullerene-based acceptors relative to the donor P3HT phase, we assume all of the solar energy absorbed by both donor and acceptor phases can generate excitons. The exciton diffusion to charge transport probability can be defined as,

$P = P_{diff} * P_{diss} * P_{perc}$, where the probability of exciton diffusion $P_{diff} = \frac{1}{N_{box}} \sum_{v} e^{\left(-\frac{d}{\varepsilon_{exciton}}\right)}$, probability of charge dissociation $P_{diss} = \frac{A_{int}}{V_{box}} * t_{int}$, probability of charge transport

$$P_{perc} = P_{P3HT} * P_{PCBM} * \frac{1}{N_{box}} \sum_{v} e^{\left(-\frac{S_A}{\varepsilon_h}\right)} * e^{\left(-\frac{S_C}{\varepsilon_e}\right)}$$

P_{P3HT} and P_{PCBM} are the corresponding percolation ratios of P3HT and PCBM phases, while d, S_A and $S_C$are respectively the shortest distances that an exciton needs to travel until it reaches an interface, a hole needs to travel to reach the anode, and that an electron needs to travel to reach the cathode. $\varepsilon_{exciton}$, ε_h and ε_e are diffusion lengths of exciton, holes and electrons, respectively; A_{int} and t_{int} are interfacial area and interface thickness; V_{box} is volume of the simulation box and N_{box} is the number of voxels after discretizing the simulation box by finite element scheme [8,38]. The stress–strain distribution is derived from the moving average calculations (sampled every 20 ps) of the p_{xx} component of the pressure tensor. UTS is calculated from the maximum engineering stress that can be obtained from the corresponding stress–strain distribution. A detailed discussion on the methods used to evaluate the objective functions are provided as supplementary information.

4. Results and discussion

A feature importance analysis based on results from our earlier efforts [9,10,20,38], as illustrated in Fig. 2A, reveals relative impact of the different design parameters on the exciton diffusion to charge transport probability. The results suggest that PCBM weight fraction is perceived as the most influential quantity affecting the morphology with ~ 60% overall contribution followed by the annealing temperature (~30%). Hence, optimizing the PCBM weight fraction and annealing temperature to establish the processing to performance relationship through the CS-CGMD framework is the key design problem. Here, the coupled CS-CGMD scheme is evaluated for three different optimization problems in accord with the parameters listed in Table 1. First, we implement the univariate CS-CGMD method where the PCBM weight fraction is optimized for enhanced exciton diffusion to charge transport probability. The results presented in Fig. 2B show an increase in exciton diffusion to charge transport probability over the several optimization generations. The globally optimal solution for PCBM weight fraction ~ 0.45 is obtained after 7 CS generations. Each objective function evaluation involves a complete CGMD simulation, where for a given PCBM weight fraction, a BHJ morphology is evolved from a ternary mixture following solvent evaporation and thermal annealing procedures. For the one-dimensional univariate problem, ~ 40 objective function evaluations are performed before the global optimum is attained. Likewise, annealing temperature also has a pronounced effect on the morphology due to molecular rearrangements of the donor polymers upon annealing [9,10]. Thus, it is desirable to implement a multivariable optimization strategy to investigate the correlation between a relatively higher dimensional parametric landscape and the blend morphology.

Fig. 2C-D present results from a bivariate (2-dimensional design space) optimization problem where PCBM weight fraction and thermal annealing temperature are concurrently optimized for the targeted exciton diffusion to charge transport probability (in principle when the probability approaches ~ 1.0, the PCE approaches ~ 100%). We compare the effect of the number of nests (n) on the overall performance of the CS optimization, by executing simulations with $n = 5$ and 10. While the ensuing effect on the efficiency of the traditional CS-CGMD method is inconclusive, the convergence of the ML-guided CS-CGMD scheme to the global optimum is accelerated with $n = 10$. The data-enabled global convergence is attained within 35 objective function evaluations, outperforming the traditional CS-CGMD scheme. For the bivariate optimization problem, the ML-guided CS-CGMD predicts an optimum PCBM weight fraction (~0.48) and thermal annealing temperature (~450 K) that effectively enhances the performance by ~ 10% from the optimum solution obtained from univariate analyses. Although the correlation between the design space and the underlying morphology is complex, we note that the global optimum determined from the ML-guided CS-CGMD concurs with earlier experimental reports [32,41].

Subsequently, we extend our data analytics model to a multi-objective optimization problem enabled by the MOCS algorithm (*i.e.*, MOCS-CGMD) [28]. The PCBM weight fraction and annealing temperature are considered to be the most influential design variables, while the objective is to concurrently examine the trends that could result in improved exciton diffusion to charge transport probability (*f1*) as well as an increased ultimate tensile strength (*f2*). Fig. 3 portrays the

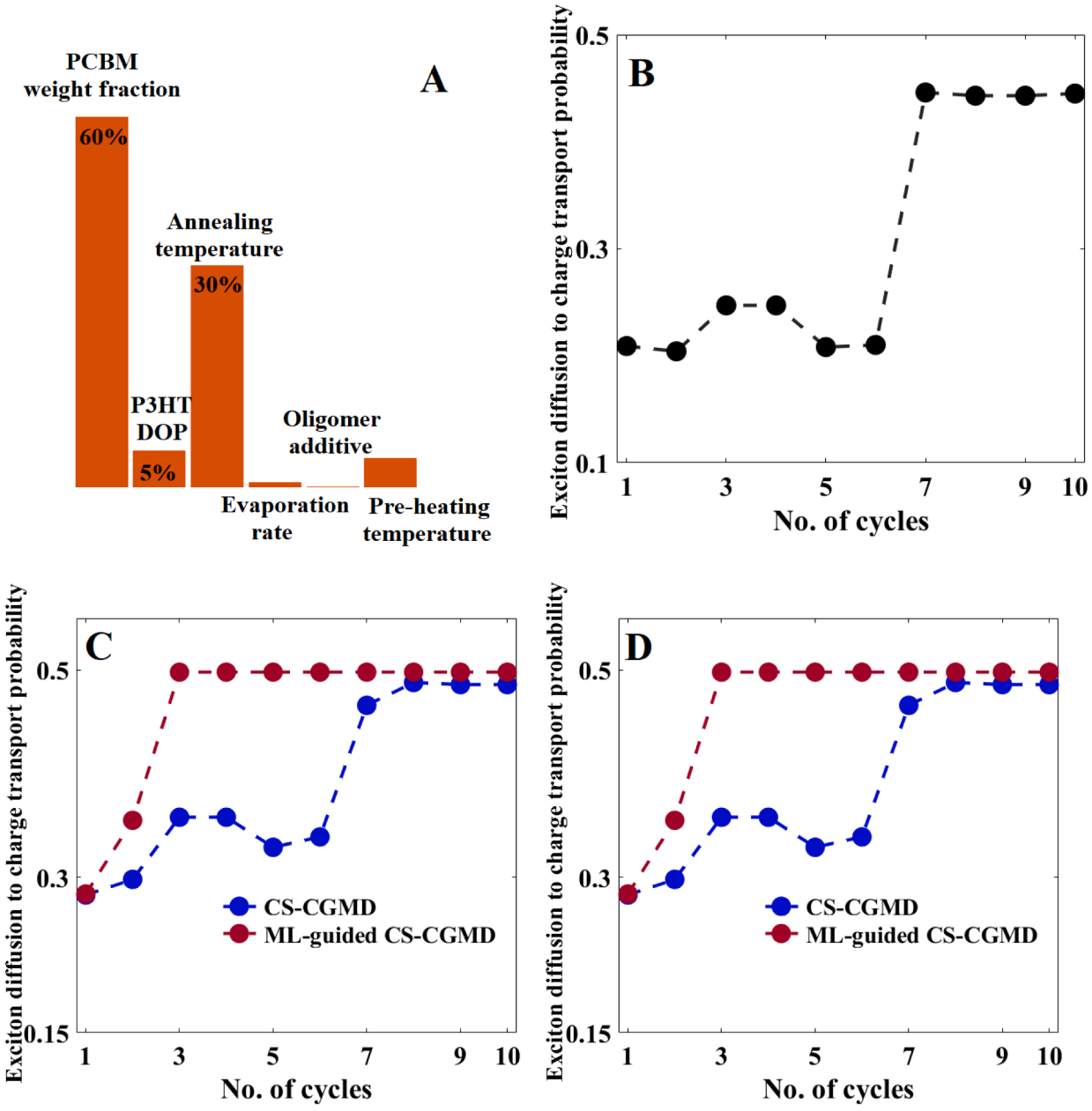

Fig. 2. A. Feature importance analysis to determine the influence of solution processing conditions on the morphology evolution. PCBM weight fraction and annealing temperature are the most influential design variables with ~ 90% contribution towards the desired performance optimization. **B.** Optimization of PCBM weight fraction as a design variable with an objective to improve exciton diffusion to charge transport probability. **C.** Bivariate optimization of PCBM weight fraction and annealing temperature for enhanced transport probability with number of nests = 5. **D.** Bivariate optimization of PCBM weight fraction and annealing temperature for enhanced transport probability with number of nests = 10. SVM assisted CS-CGMD outperforms the traditional CS-CGMD irrespective of the number of nests.

Table 1
Design variables and bounds for the CS-CGMD optimization framework. Upper and lower bounds for the different design variables are adopted from previous experimental and computational efforts [10,20,32,41–43].

Problem Classification	Design variable	Upper bound	Lower bound	Switching parameter	No. of nests	No. of generations
Univariate	PCBM	0.15	0.85	0.2	5	10
Bivariate	PCBM	0.15	0.85	0.2	5, 10	10
	Annealing temperature	323 K	473 K			
Bivariate multi-objective	PCBM	0.15	0.85	0.2	10	10
	Annealing temperature	323 K	473 K			

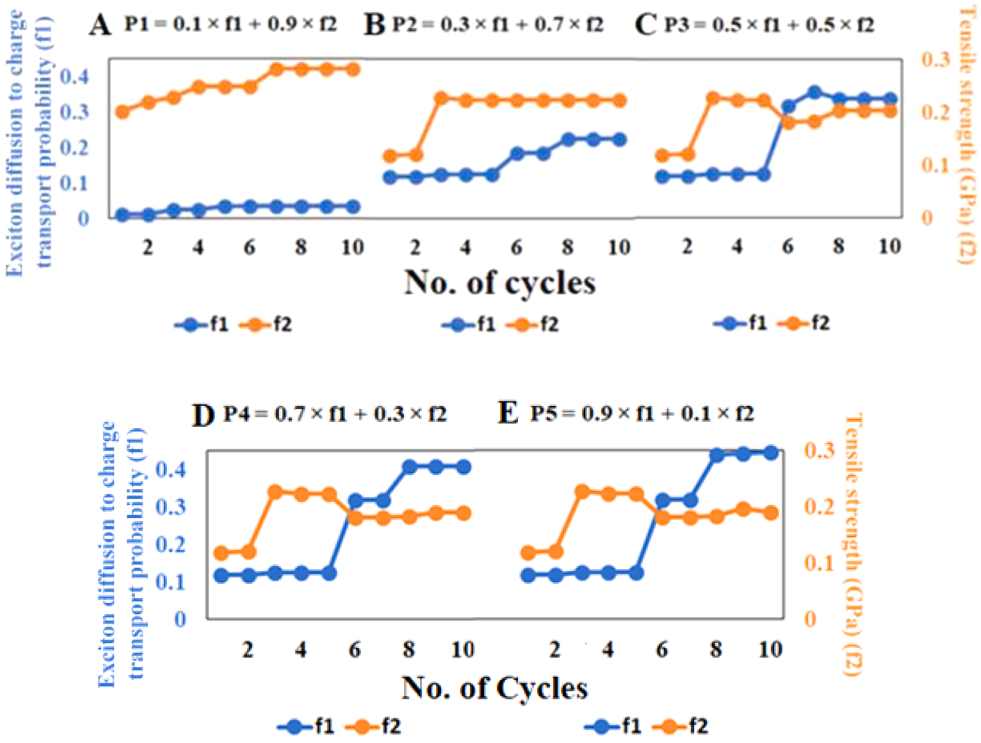

Fig. 3. A-E. Bivariate optimization of PCBM weight fraction and annealing temperature with multiple objective functions such as the exciton diffusion to charge transport probability (f1) and ultimate tensile strength (f2) during the SVM assisted CS-CGMD generations. Five optimization scenarios are selected separately with different preferences (weights) set for two objective functions to generate the Pareto front: **A.** 10% exciton diffusion to charge transport probability (f1) and 90% tensile strength (f2); **B.** 30% f1 and 70% f2; **C.** 50% f1 and f2; **D.** 70% f1 and 30% f2; **E.** 90% f1 and 10% f2.

progression of two objective functions during the MOCS-CGMD optimization generations.

Results from Fig. 3A illustrate the convergence of ultimate tensile strength to attain the global solution while the charge transport probability is compromised. On the other hand, in Fig. 3E the trend in the progression is completely reversed due to the trade-off between the two objective functions. The approximated Pareto front generated by 5 subservient solutions after 10 generations of optimization run, leading to ~ 500 objective function evaluations, is shown in Fig. 4A. Predictions from the SVM assisted model over 10 generations of MOCS runs reveal

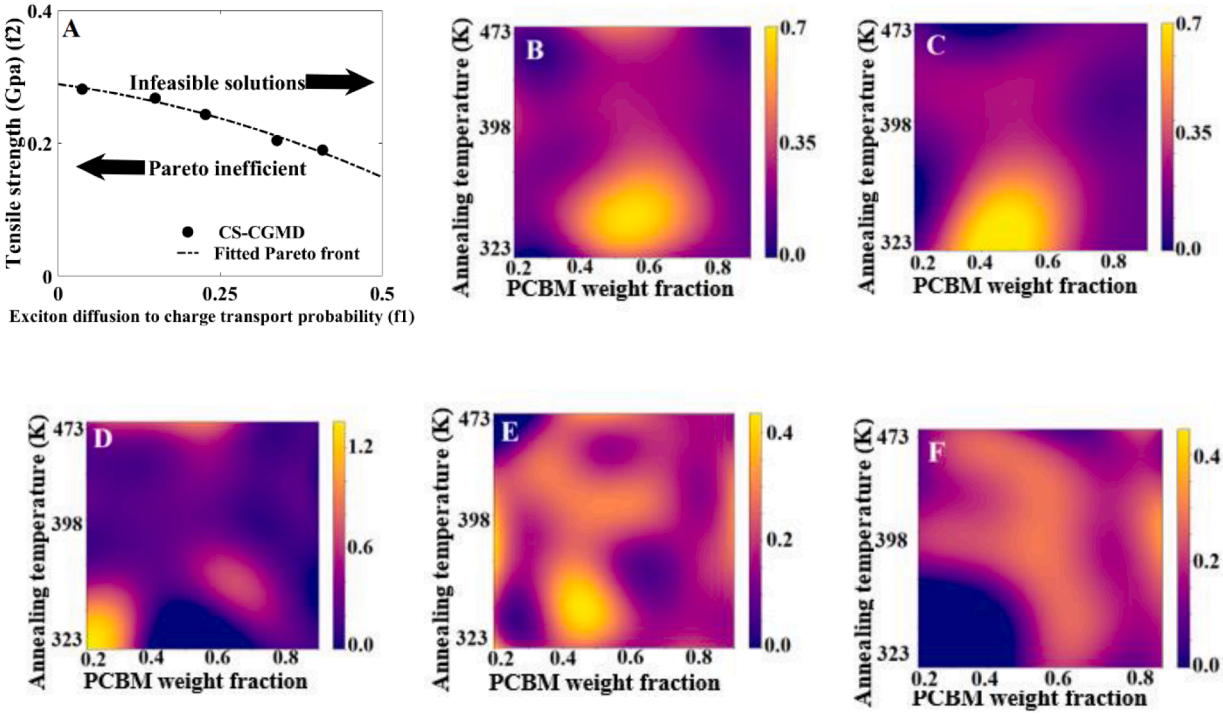

Fig. 4. A. Generated Pareto optimal solutions from SVM assisted CS-CGMD scheme and fitted Pareto front as a function of the two objective functions. **B-F.** Support vector regression (SVR) with radial basis function (RBF) satisfies the objective function trained on the 500 CGMD simulations generated after 10 generations of SVM assisted CS-CGMD optimization: **B.** 10% exciton diffusion to charge transport probability (f1) and 90% tensile strength (f2); **C.** 30% f1 and 70% f2; **D.** 50% f1 and f2; **E.** 70% f1 and 30% f2; **F.** 90% f1 and 10% f2.

the Pareto optimality situation. We find that no individual solutions from the Pareto front can be considered as the global optimum for one of the targeted properties without compromising the other. Fig. 4B-F illustrate the converged ROIs on the 2-dimensional design landscape for different combinations of the targeted objective as a function of PCBM weight fraction and annealing temperature. When mechanical strength is prioritized, in lieu of the exciton diffusion to charge transport probability, as the desired objective function (Fig. 4B), the global optimum is identified around PCBM weight fraction between 0.4 and 0.6 and annealing temperature ~ 340 K. In contrast, when the exciton diffusion to charge transport probability is considered as the preferred objective function (Fig. 4F) suppressing the need for an enhanced tensile strength, the global optimum migrates around new ROI (PCBM weight fraction < 0.5 and annealing temperature ~ 420 K).

The predicted trends intuitively correlate to the molecular arrangements of the annealed polymers. With an increase in annealing temperature, the polymers tend to align themselves with each other enhancing the crystallinity and hence the overall charge transport through the blend. Although the crystalline domains inside a pure P3HT phase tend to increase the ultimate tensile strength, P3HT:PCBM blend exhibits increased strength until the PCBM weight fraction approaches a threshold ~ 0.6 [20]. Thus, it is evident that the choice of the preferred objective function drives the converged ROIs across the vast design landscape. Fig. 4C-E reveal the migration of the ROIs and the global optimum when the objective functions are prioritized according to their corresponding weights. Based on these results, it is evident that an ideal OPV BHJ layer comprises of a trade-off between the performance and mechanical strength, which necessitates a robust predictive modeling to establish PSP relationship across the vast landscape of design parameters.

5. Conclusion

In summary, we employ CGMD simulations coupled with the metaheuristic Cuckoo Search optimization (CS-CGMD) to correlate solution processing parameters with the morphological evolution consisting of electron-donor P3HT and electron-acceptor PCBM molecules. A ML-guided approach to augment the traditional CS-CGMD is observed to significantly enhance the convergence of the 2-dimensional design space to attain the global optimum solutions. Based on the success of the ML-guided approach in contrast to the traditional optimization scheme, we extend the machine learned metaheuristic search algorithm to define a multi-objective optimization framework leveraging CGMD simulations (MOCS-CGMD) on the fly, to attain faster convergence to the global solution. Results from the optimization run based on ~ 500 objective function evaluations reveal a Pareto optimality situation consisting of subordinate solutions. While an increase in annealing temperature is observed to enhance the exciton diffusion to charge transport probability, a PCBM weight fraction between 0.4 and 0.6 is recommended for increased tensile strength of the underlying blend morphology. Thus, the SVM assisted MOCS-CGMD optimization framework, implemented in this investigation, demonstrates remarkable capability to identify complex correlations of the vast design landscape with the targeted properties and can be integrated with high-throughput framework for novel materials discovery to accelerate the design of efficient organic solar cells and quasirandom nanostructured materials.

CRediT authorship contribution statement

Joydeep Munshi: Methodology, Coding, Computational modeling, Manuscript preparation. **Wei Chen:** Discussion of results, Manuscript editing. **TeYu Chien:** Discussion of results, Manuscript editing. **Ganesh Balasubramanian:** Conceptualization, Supervision, Review and Editing.

Declaration of Competing Interest

The authors declare that they have no known competing financial interests or personal relationships that could have appeared to influence the work reported in this paper.

Acknowledgments

This material is based on the work supported by the National Science Foundation (NSF) under Award Nos. CMMI-1662435, 1662509 and 1753770 (the latter includes support from a supplement for data science related CMMI research activities). JM and GB acknowledge the allocation of leadership class computing time on Frontera (at the Texas Advanced Computing Center (TACC) in The University of Texas at Austin) to perform the simulations and support through the NSF award # OAC-2031682. Any opinions, findings, conclusions or recommendations expressed in this material are those of the authors' and do not necessarily reflect the views of the NSF.

Data Availability

The raw/processed data required to reproduce these findings cannot be shared at this time as the data also forms part of an ongoing study.

Appendix A. Supplementary data

Supplementary data to this article can be found online at https://doi.org/10.1016/j.commatsci.2020.110119.

References

[1] S. Günes, H. Neugebauer, N.S. Sariciftci, Conjugated Polymer-Based Organic Solar Cells, Chem. Rev. 107 (4) (2007) 1324–1338.
[2] B.C. Thompson, J.M.J. Fréchet, Polymer-Fullerene Composite Solar Cells, Angew. Chem. Int. Ed. 47 (1) (2008) 58–77.
[3] L.-M. Chen, et al., Recent Progress in Polymer Solar Cells: Manipulation of Polymer: Fullerene Morphology and the Formation of Efficient Inverted Polymer Solar Cells, Adv. Mater. 21 (14–15) (2009) 1434–1449.
[4] M.C. Scharber, N.S. Sariciftci, Efficiency of bulk-heterojunction organic solar cells, Prog. Polym. Sci. 38 (12) (2013) 1929–1940.
[5] R. Alessandri, et al., Bulk Heterojunction Morphologies with Atomistic Resolution from Coarse-Grain Solvent Evaporation Simulations, J. Am. Chem. Soc. 139 (10) (2017) 3697–3705.
[6] J.-M.-Y. Carrillo, et al., New insights into the dynamics and morphology of P3HT: PCBM active layers in bulk heterojunctions, PCCP 15 (41) (2013) 17873–17882.
[7] C.-K. Lee, C.-W. Pao, C.-W. Chu, Multiscale molecular simulations of the nanoscale morphologies of P3HT:PCBM blends for bulk heterojunction organic photovoltaic cells, Energy Environ. Sci. 4 (10) (2011) 4124–4132.
[8] U.F., Ghumman, et al., A Spectral Density Function Approach for Design of Organic Photovoltaic Cells, in ASME IDETC/CIE Design Automation Conference. 2018, ASME: Quebec City, Quebec, Canada.
[9] J. Munshi, et al., Composition and processing dependent miscibility of P3HT and PCBM in organic solar cells by coarse-grained molecular simulations, Comput. Mater. Sci. 155 (2018) 112–115.
[10] J. Munshi, et al., Solution Processing Dependent Bulk Heterojunction Nanomorphology of P3HT/PCBM Thin Films, ACS Appl. Mater. Interfaces 11 (18) (2019) 17056–17067.
[11] G. Li, R. Zhu, Y. Yang, Polymer solar cells, Nat. Photonics 6 (2012) 153.
[12] M.R. Lee, et al., Solar Power Wires Based on Organic Photovoltaic Materials, Science 324 (5924) (2009) 232–235.
[13] M. Kaltenbrunner, et al., Ultrathin and lightweight organic solar cells with high flexibility, Nat. Commun. 3 (2012) 770.
[14] X. Che, et al., High fabrication yield organic tandem photovoltaics combining vacuum- and solution-processed subcells with 15% efficiency, Nat. Energy 3 (5) (2018) 422–427.
[15] Y. Cui, et al., Organic photovoltaic cell with 17% efficiency and superior processability, Natl. Sci. Rev. 7 (7) (2020) 1239–1246.
[16] C.Y. Yang, A.J. Heeger, Morphology of composites of semiconducting polymers mixed with C60, Synth. Met. 83 (2) (1996) 85–88.
[17] N. Stingelin-Stutzmann, et al., Organic thin-film electronics from vitreous solution-processed rubrene hypereutectics, Nat. Mater. 4 (2005) 601.
[18] M. Jørgensen, K. Norrman, F.C. Krebs, Stability/degradation of polymer solar cells, Sol. Energy Mater. Sol. Cells 92 (7) (2008) 686–714.
[19] A.T. Kleinschmidt, S.E. Root, D.J. Lipomi, Poly(3-hexylthiophene) (P3HT): fruit fly or outlier in organic solar cell research? J. Mater. Chem. A 5 (23) (2017) 11396–11400.

[20] J. Munshi, et al., Elasto-morphology of P3HT:PCBM bulk heterojunction organic solar cells, Soft Matter (2020).
[21] S.E. Root, et al., Predicting the Mechanical Properties of Organic Semiconductors Using Coarse-Grained Molecular Dynamics Simulations, Macromolecules 49 (7) (2016) 2886–2894.
[22] Y. Liu, C. Storey, Efficient generalized conjugate gradient algorithms, part 1: Theory, J. Optim. Theory Appl. 69 (1) (1991) 129–137.
[23] S. Ruder, An overview of gradient descent optimization algorithms, 2016.
[24] S.N. Sivanandam, S.N. Deepa, Genetic Algorithm Optimization Problems, in Introduction to Genetic Algorithms, in: S.N. Sivanandam, S.N. Deepa, (Eds.) 2008, Springer Berlin Heidelberg: Berlin, Heidelberg. pp. 165-209.
[25] J. Kennedy, R. Eberhart. Particle swarm optimization. in Proceedings of ICNN'95 - International Conference on Neural Networks, 1995.
[26] X. Yang, D. Suash Cuckoo Search via Lévy flights in 2009 World Congress on Nature & Biologically Inspired Computing (NaBIC), 2009.
[27] X.-S. Yang, Review of meta-heuristics and generalised evolutionary walk algorithm, Int. J. Bio-Inspir. Comput. 3 (2) (2011) 77–84.
[28] X.-S. Yang, S. Deb, Multiobjective cuckoo search for design optimization, Comput. Oper. Res. 40 (6) (2013) 1616–1624.
[29] D.C. Lahti, Evolution of bird eggs in the absence of cuckoo parasitism, PNAS 102 (50) (2005) 18057.
[30] M. Jamil, H. Zepernick, X. Yang, Levy Flight Based Cuckoo Search Algorithm for Synthesizing Cross-Ambiguity Functions MILCOM 2013–2013 IEEE Military Communications Conference, 2013.
[31] A. Sharma, et al., Cuckoo searching optimal composition of multicomponent alloys by molecular simulations, Scr. Mater. 130 (2017) 292–296.
[32] B. Cao, et al., How To Optimize Materials and Devices via Design of Experiments and Machine Learning: Demonstration Using Organic Photovoltaics, ACS Nano 12 (8) (2018) 7434–7444.
[33] Pedregosa, F., et al., Scikit-learn: Machine Learning in Python. J. Mach. Learn. Res., 2011. 12(null): p. 2825–2830.
[34] S.J. Marrink, D.P. Tieleman, Perspective on the Martini model, Chem. Soc. Rev. 42 (16) (2013) 6801–6822.
[35] L. Monticelli, On Atomistic and Coarse-Grained Models for C60 Fullerene, J. Chem. Theory Comput. 8 (4) (2012) 1370–1378.
[36] E. Panizon, et al., MARTINI Coarse-Grained Models of Polyethylene and Polypropylene, J. Phys. Chem. B 119 (25) (2015) 8209–8216.
[37] M. Vögele, C. Holm, J. Smiatek, Coarse-grained simulations of polyelectrolyte complexes: MARTINI models for poly(styrene sulfonate) and poly (diallyldimethylammonium), J. Chem. Phys. 143 (24) (2015), 243151.
[38] J. Munshi, et al., Effect of polydispersity on the bulk-heterojunction morphology of P3HT:PCBM solar cells, J. Polym. Sci., Part B: Polym. Phys. 57 (14) (2019) 895–903.
[39] M.J. Abraham, et al., GROMACS: High performance molecular simulations through multi-level parallelism from laptops to supercomputers, SoftwareX 1–2 (2015) 19–25.
[40] W. Humphrey, A. Dalke, K. Schulten, VMD - Visual Molecular Dynamics, J. Molec. Graphics 14 (1996) 33–38.
[41] D. Chen, et al., P3HT/PCBM Bulk Heterojunction Organic Photovoltaics: Correlating Efficiency and Morphology, Nano Lett. 11 (2) (2011) 561–567.
[42] C.J. Brabec, et al., Influence of blend microstructure on bulk heterojunction organic photovoltaic performance, Chem. Soc. Rev. 40 (3) (2011) 1185–1199.
[43] C.-K. Lee, C.-W. Pao, Nanomorphology Evolution of P3HT/PCBM Blends during Solution-Processing from Coarse-Grained Molecular Simulations, J. Phys. Chem. C 118 (21) (2014) 11224–11233.